This is a repository copy of *Non-polar (11-20) GaN metal-semiconductor-metal photo-detectors with superior performance on silicon*.

White Rose Research Online URL for this paper:
https://eprints.whiterose.ac.uk/160839/

Version: Published Version

Article:

Nonpolar (11$\bar{2}$0) GaN Metal−Semiconductor−Metal Photodetectors with Superior Performance on Silicon

Yuefei Cai,[#] Shuoheng Shen,[#] Chenqi Zhu, Xuanming Zhao, Jie Bai, and Tao Wang*

Cite This: ACS Appl. Mater. Interfaces 2020, 12, 25031−25036

Read Online

ACCESS | Metrics & More | Article Recommendations | SI Supporting Information

ABSTRACT: This article reports a nonpolar GaN metal−semiconductor−metal (MSM) photodetector (PD) with an ultrahigh responsivity and an ultrafast response speed in the ultraviolet spectral region, which was fabricated on nonpolar (11$\bar{2}$0) GaN stripe arrays with a major improvement in crystal quality grown on patterned (110) silicon substrates by means of using our two-step processes. Our nonpolar GaN MSM-PD exhibits a responsivity of 695.3 A/W at 1 V bias and 12628.3 A/W at 5 V bias, both under 360 nm ultraviolet illumination, which are more than 20 times higher and 4 orders of magnitude higher compared to the current state-of-the-art photodetector, respectively. The nonpolar GaN MSM-PD displays a rise time and a fall time of 66 and 43 μs, respectively, which are 3 orders of magnitude faster compared to the current state-of-the-art photodetector.

KEYWORDS: nonpolar GaN, photodetector, responsivity, response time, ultraviolet, silicon substrates
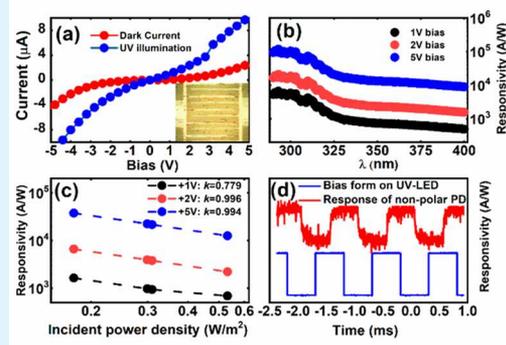
INTRODUCTION

Developing ultraviolet (UV) photodetectors (PDs) that can find a wide range of applications, such as flame sensors, atmospheric ozone detection, space communications, and biophotonics,[1−7] is a subject facing increasing interest. Given that GaN exhibits a direct band gap structure with its band gap (3.43 eV) in the UV spectral region, it is expected that GaN-based UV PDs exhibit superior performance to Si-based PDs in the UV spectral region (Si has an indirect band structure with a 1.1 eV band gap). Generally speaking, both crystallographic orientation and surface polarity also play a critical role in determining the performance of a photodetector.[8] Current GaN optoelectronics, which is overwhelmingly dominated by c-plane GaN, exhibits inherent polarization, one of the fundamental limitations leading to GaN PDs with reduced performance in terms of efficiency and response speed; however, nonpolar GaN intrinsically exhibits zero polarization effects. As a result, nonpolar GaN-based UV PDs are supposed to demonstrate much higher efficiency and much faster response than their c-plane counterparts.[9−14]

It is worth highlighting that the crystal quality of nonpolar GaN grown on widely used sapphire substrates or silicon substrates is far from a device requirement, normally showing a very broad full width at half-maximum (fwhm) of ~0.5−0.6° of its X-ray diffraction (XRD) rocking curve,[9−14] whereas the typical value of standard c-plane GaN on sapphire or silicon is less than 0.1°. This indicates a very high density of defects in nonpolar GaN, thus leading to a slow response of nonpolar PDs with a rise time ranging from 0.046 to 17.5 s and a fall-time ranging from 0.075 to 20.5 s, heavily depending on the crystal quality,[15] whereas the rise time and the fall time of c-plane GaN are typically 10 and 30−59 ms, respectively.[16,17] Clearly, there exists a great potential for achieving superior performance GaN UV PDs if a step change in the crystal quality of nonpolar GaN can be obtained.

The homoepitaxial growth of nonpolar GaN is ideal, but it is impractical as a result of the lack of native substrates with affordable costs. Therefore, it is crucial to explore a new method for obtaining nonpolar GaN heteroepitaxially grown on industry-compatible substrates, that is, sapphire or silicon. For these two kinds of substrates, it is crucially important to overcome a number of great challenges due to the huge lattice mismatch between sapphire or silicon and GaN. It is worth highlighting that the situation becomes even worse for silicon substrates compared to that for sapphire substrates. The growth of GaN PDs on silicon substrates is drawing increasing attention, partially driven by an increasing demand for integrating III-nitride compound semiconductors with silicon technologies by taking advantage of their respective merits, which has been accepted to play a critical role in fabricating future photonic integrated circuits.[18,19] However, unlike sapphire substrates, it is almost impossible to grow nonpolar
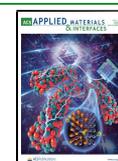
GaN on any planar silicon substrate because of the incompatibility of the epitaxial relationship between nonpolar GaN and Si substrate with any orientation. So far, nonpolar GaN on silicon is mainly obtained via selective growth on patterned silicon substrates.[20,21] For instance, $(11\bar{2}0)$ nonpolar GaN can be achieved by means of employing selective growth on patterned (110) silicon, where the formed {111} Si facets are exposed for selective growth. In that case, there exist two extra major challenges, namely, Ga meltback and cracking. For the former, in the case of the growth of c-plane GaN on planar (111) silicon, a thick AlN buffer layer is initially grown, effectively separating GaN subsequently grown on the AlN buffer from the silicon and thus eliminating Ga meltback. However, nonpolar GaN has to be selectively grown on an inclined {111} facet on patterned (110) silicon, and thus the risk for the generation of Ga meltback is significantly enhanced because only a thin AlN buffer layer is allowed. Otherwise, nonpolar GaN growth based on the selective growth mechanism is ruined if a thick AlN buffer layer is used.

Furthermore, the huge mismatch in thermal expansion coefficient between GaN and silicon (∼54%) potentially leads to severe cracking, which cannot be eliminated by using the standard strain-engineering approaches widely used for the growth of c-plane GaN on planar (111) silicon, namely, using thick AlGaN layers with graded Al content prior to the growth of GaN.[22,23] As nonpolar GaN needs to be selectively grown on patterned silicon, such selective growth will be stopped if thick AlGaN layers are grown prior to the deposition of GaN.

In recent decades we have developed a number of cost-effective overgrowth approaches to achieve semipolar and nonpolar GaN with a major improvement in crystal quality on sapphire.[24−27] We have further extended these approaches to the growth on silicon substrates. In this paper, we have demonstrated cracking-free and stripe-arrayed nonpolar $(11\bar{2}0)$ GaN with a major improvement in crystal quality on patterned (110) silicon. On the basis of the high-quality nonpolar GaN with a stripe configuration, a nonpolar GaN metal−semiconductor−metal photodiode (MSM-PD) has been fabricated, demonstrating superior performance in comparison to the current state-of-the-art photodetector in terms of both responsivity and response speed. Our nonpolar GaN MSM-PD exhibits an extremely high responsivity, which is 1 order of magnitude higher than the current state of-the art photodetector, and an extremely fast response, which is 3 orders of magnitude faster than the current state of-the art photodetector.

RESULTS AND DISCUSSION

Figure 1 schematically illustrates our detailed procedures for patterning (110) Si substrate, which include transferring stripy patterns onto stripy SiO2 masks on the silicon substrate using a conventional photolithography technique, then a dry-etching method (Figure 1a−d), and finally chemical wet-etching processes (Figure 1e,f). Because of the naturally anisotropic properties of silicon, chemical etching almost stops once the etching front meets {111} facets. Consequently, the {111} Si facets including the $(1\bar{1}1)$ and $(\bar{1}1\bar{1})$ planes are finally formed in addition to the partially unetched top (110) facets on which the SiO2 stripy masks protect the silicon underneath from chemical etching. The etching depth can be controlled by etching time. Finally, all the SiO2 stripy masks on top of the (110) facet are removed by HF.
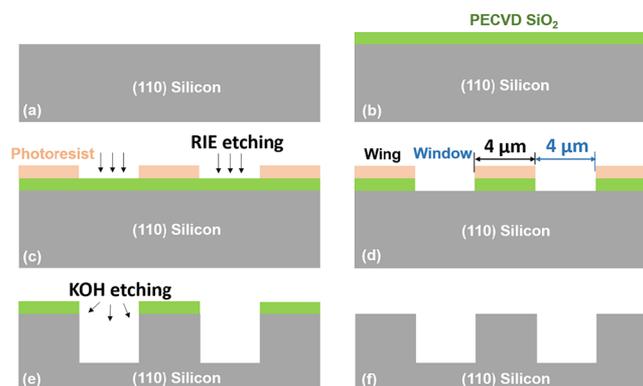
Figure 1. Schematics for our procedure of the fabrication of a patterned (110) Si substrate. (a) (110) silicon substrate; (b) SiO2 deposited on a silicon substrate by PECVD; (c) formation of photoresist stripe patterns by a standard photolithography technique; (d) formation of SiO2 stripe patterns by dry-etching processes; (e) KOH wet etching to form patterned silicon with SiO2 masks; and (f) final patterned silicon substrate after SiO2 mask removal by HF.

Afterward, the patterned (110) silicon substrate is reloaded into a metal−organic vapor-phase epitaxy (MOVPE) chamber. With use of a similar procedure for the growth of standard c-plane GaN on planar (111) silicon substrates, a 400 nm AlN buffer layer is initially grown in order to cover all of the facets very well, aiming at eliminating Ga meltback during the followed GaN overgrowth process at a high temperature, as schematically illustrated in Figure 2a.
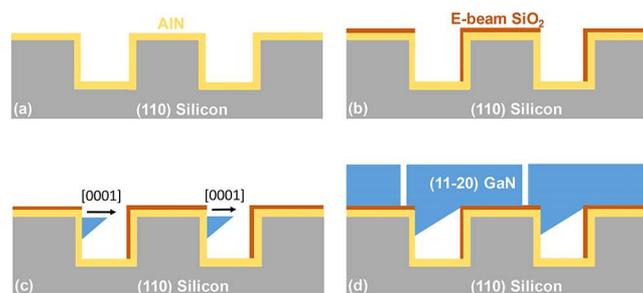
Figure 2. Schematics of our nonpolar $(11\bar{2}0)$ GaN growth processes on the patterned (110) Si. (a) AlN deposition; (b) E-beam SiO2 sputtering; (c) initial growth of GaN on {111} facets; and (d) formation of nonpolar GaN stripes.

To perform selective overgrowth, we need to selectively deposit a thin SiO2 film, which covers all other facets but leaves the $(1\bar{1}1)$ facets to be exposed only as indicated in Figure 2b. For this purpose, an angle shadow deposition technique is employed by a standard electron beam deposition technique. Basically, the sample is mounted at a particular angle with respect to the SiO2 beam, where the inclined angle has been optimized so that SiO2 can be deposited on all the other facets except the $(1\bar{1}1)$ facet.

Figure 2c,d schematically illustrates the evolution of an overgrowth process. The overgrowth initially takes place on the exposed $(1\bar{1}1)$ facets only and then extends over the SiO2 masks on the (110) facets. Eventually, the nonpolar $(11\bar{2}0)$ stripes with a flat surface and straight sidewalls are formed. A V/III ratio and growth temperature are two key parameters for controlling lateral or vertical growth rates, which eventually affect the morphology of the nonpolar GaN stripes. Generally

speaking, an increase in growth temperature helps increase a later growth rate. A decrease in the V/III ratio also gives rise to an increase in lateral growth rate. An increased lateral growth rate facilitates the formation of a flat surface.

Figure 3a,b shows the typical plane-view and cross-sectional scanning electron microscopy (SEM) images of the nonpolar
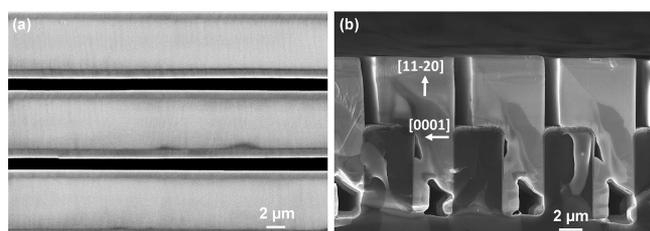
Figure 3. Plane-view (a) and cross-sectional (b) SEM images of our nonpolar GaN stripe arrays grown on the patterned (110) Si.

$(11\bar{2}0)$ GaN stripe arrays, confirming the aforementioned overgrowth process; namely, the overgrowth initially takes place on the exposed $(1\bar{1}1)$ facet only and then extends over the SiO_2 masks. No Ga meltback has been observed, confirming that the Ga meltback can be effectively suppressed by our growth method, even at a high temperature above 1200 °C.

Detailed X-ray diffraction (XRD) measurements have been performed to characterize the crystal quality by means of measuring the full width at half-maximum (fwhm) of XRD rocking curves as shown in Figure 4a, which are compared to
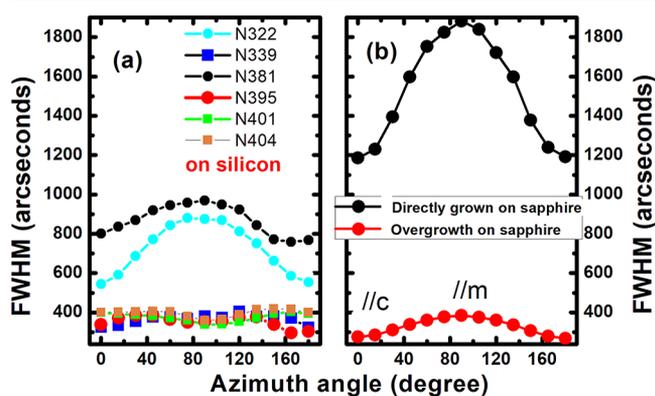
Figure 4. fwhm of XRD rocking curves as a function of an azimuthal angle for (a) our nonpolar GaN stripe arrays grown on the patterned (110) Si under different conditions (V/III ratio and growth temperature), and (b) standard nonpolar GaN directly grown on r-plane sapphire and our well-established nonpolar GaN overgrown on a patterned template on r-plane sapphire.

our nonpolar GaN overgrown on patterned nonpolar GaN templates on r-plane sapphire, which have been well-established by our team as shown in Figure 4b. By optimization of our growth conditions (V/III ratio and temperatures; for details, please refer to Table S1 in the Supporting Information), the fwhm's of the XRD rocking curves along the mutually perpendicular c- and m-directions are 325 and 380 arcsec, respectively, which are among the best values reported,[25] whereas standard nonpolar GaN directly grown on foreign substrates displays a typical fwhm of an XRD rocking curve of 1908−3309 arcsec.[10] Figure 4b also provides

the fwhm's of the XRD rocking curves of standard nonpolar GaN directly grown on sapphire.

Further data to prove the high crystal quality includes low-temperature photoluminescence (PL) measurements, which are very useful for investigating basal stacking faults (BSF) in nonpolar GaN.[28] Figure 5 shows the typical PL spectrum of
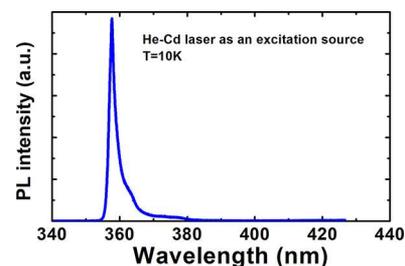
Figure 5. Photoluminescence spectra of our nonpolar $(11\bar{2}0)$ GaN stripe arrays grown on the patterned (110) silicon substrate, measured at 10 K.

our $(11\bar{2}0)$ nonpolar GaN measured at 10 K, where the sample is excited by using a 325 nm He−Cd laser. Figure 5 shows an emission peak with very strong intensity at 357.7 nm from the band-edge emission and a very weak shoulder at 363 nm from the BSF-related emission,[21,28] which are similar to the current state-of-the-art device for nonpolar or semipolar GaN overgrown on patterned templates on sapphire.[21] This indicates a very low BSF density.

A MSM-PD has been subsequently fabricated on high-quality nonpolar GaN with a stripy configuration. Detailed characterizations have been conducted on the MSM-PD. The inset of Figure 6a shows the image of our MSM-PD devices with an interdigitated finger configuration, where the finger Schottky metal contact consists of Ti/Ai/Ti/Au (50/200/50/50 nm) and the spacing between two neighboring fingers is 30 μm. All of the finger metal contacts are parallel to the stripe pattern direction. Photoresponsivity measurements have been carried out by a standard photoresponse testing system. We have measured 18 MSM-PD devices in total, which have been fabricated in the same batch, and the standard deviation is ±3%.

Figure 6a shows the current−voltage (I−V) characteristic of our MSM-PD with an active area of $284 \times 393 \ \mu m^2$ under dark and UV-illumination conditions.

Figure 6b shows the typical responsivity of our MSM-PDs as a function of wavelength measured under different biases (1, 2, and 5 V). For details, Figure 6b shows that our MSM-PD demonstrates a high responsivity of 695.30 A/W under 360 nm UV illumination typically at 1 V bias, which is more than 20 times higher than the current state-of-the art device. This value increases to 2218.53 A/W at 2 V bias and to 12628.25 A/W at 5 V bias, which is 4 orders of magnitude higher than the current state-of-the-art device.[13] Such a high responsivity can be attributed to a step-change in the crystal quality of our nonpolar GaN as shown in Figure 4, which greatly increases the mobility of the carriers and thus reduces the transit time of photogenerated carriers.

After careful examination of Figure 6b, it can be found that the ratio of responsivity in the UV region to that in the blue region (below the GaN band gap) is about 10. This is due to the trenches between nonpolar GaN stripes just covered by the AlN buffer layer directly on silicon, where the silicon within
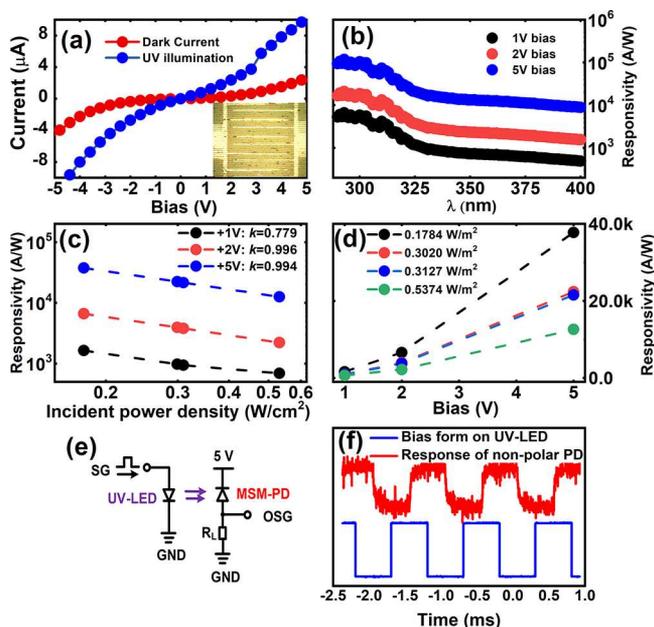
Figure 6. (a) Current−voltage (I−V) characteristic measured under dark and UV illumination conditions. Inset: Microscope image of the nonpolar GaN MSM-PD. (b) Responsivity of our nonpolar GaN MSM-PD as a function of wavelength in the UV spectral region measured under different biases (1, 2, and 5 V). (c) Responsivity as a function of incident power density under 360 nm illumination at different biases. (d) Responsivity as a function of bias under 360 nm illumination. (e) Schematics for our response time testing system. (f) Response waveforms of our nonpolar PD under modulated UV-LED illumination at 2 kHz.

the trenches contributes to the absorption with a photon energy lower than the GaN band gap. This also rules out the possibility of light absorption via point defects in the GaN layer or traps at the interface of the Ti/GaN Schottky junctions,[29] further confirming the high quality of our nonpolar GaN

Figure 6c presents the responsivity of our MSM-PDs as a function of incident power density (labeled as P) under 360 nm illumination conditions measured at different biases, demonstrating that they follow the standard P^{-k} law. k has been obtained as 0.78−1, which is similar to that found in another report.[30] This indicates a photoconductive internal gain, explained as a modulation mechanism for the conductive

volume of the layer. Photogenerated carriers are separated by potential barriers, induced as a result of dislocation-related band bending either on the surface or within the bulk layer. Moreover, the potential barriers also determine the carrier recombination and carrier capture, leading to an intrinsic nonexponential recovery process. Bias-dependent responsivity measurements as shown in Figure 6d further confirm the photoconductive mechanism.

To measure the response time of our MSM-PD, a commercial UV-LED serving as an UV illumination source at ∼360 nm has been directly modulated by a square waveform generated by a signal generator (SG) at 1 kHz with an amplitude of 3.2 V and an offset of 2 V, whereas our MSM-PD has been used to detect the modulated UV light. Figure 6e schematically illustrates the response time measurement system, where our MSM-PD is biased at 5 V and a 2 kΩ load resistor (R_L) is used.

Figure 6f displays both the input signal (i.e., the voltage waveform applied on UV-LED) and the response waveform of our MSM-PD. The rise and fall current can be expressed by eq 1 and 2 provided below:[14]

$$I(t) = I_{dark} + A\left[1 - \exp\left(-\frac{t - t_0}{t_{rise}}\right)\right] \quad (1)$$

$$I(t) = I_{dark} + A\left[\exp\left(-\frac{t - t_0}{t_{fall}}\right)\right] \quad (2)$$

where I_{dark} is the dark current, A is a scaling constant, and t_0 is the time for switching on/off the UV light source. t_{rise} and t_{fall} is the rise and fall time, respectively, and can be extracted by fitting.

With use of a standard exponential function for fitting (for details, please refer to Figure S1 in the Supporting Information), the rise time and the fall time of our MSM-PDs are 66 and 43 μs, which are 3 orders of magnitude faster in comparison to those using the current state-of-the-art nonpolar GaN PDs.[9−14] The fast build-up and recovery time also indicate a great reduction in the number of shallow and deep traps in our nonpolar GaN, resulting in the shorter relaxation time.[15] This can be attributed to a step-change crystal quality of our nonpolar GaN. Table 1 shows our results benchmarked against the current state-of-the-art nonpolar PDs in terms of performance, demonstrating that the crystal quality of nonpolar GaN (evaluated by the fwhm's of XRD rocking

Table 1. Our Nonpolar MSM-PD and the Current State-of-the-Art Device in Terms of Their Performance and Crystal Quality

ref	year	materials	substrates	XRD rocking curve fwhm (arcsec)	applied bias (V)	responsivity (A/W)	rise time (s)	fall time (s)
this work	2019	(11$\bar{2}$0) GaN	(110) silicon	325 along [0002] 380 along [1$\bar{1}$00]	1	695.3	0.000066	0.000043
10	2019	(11$\bar{2}$0) GaN	r-sapphire	1908 2755 3309	1 1 1	25.243 25.32 4.42	0.257 0.222 0.163	1.99 2.1 1.98
11	2018	(11$\bar{2}$0) GaN	r-sapphire	2160 along [0002] 6480 along [1$\bar{1}$00]	1	1.8803	0.21	1.2
13	2018	(11$\bar{2}$0) GaN	LaAlO$_3$	756 along [11$\bar{2}$0] 1476 along [10$\bar{1}$1]	5	1.35	0.046	0.075
12	2017	(11$\bar{2}$0) GaN	r-sapphire	1764 along [11$\bar{2}$0]	5	0.34	0.28	0.45
9	2015	(11$\bar{2}$0) GaN	r-sapphire		2	0.155	6	15
14	2014	(10$\bar{1}$0)GaN	m-sapphire	2336 along [0001] 3751 along [12$\bar{1}$0]	2	0.407	17.5	25

curves), plays a vital role in obtaining high performance in terms of response time.

For further comparison, we have also measured a typical *c*-plane GaN MSM-PD grown on (111) silicon, which was processed in the same batch as our nonpolar GaN MSM-PD and was measured under identical conditions. The *c*-plane GaN MSM-PD shows a rise time and a fall time of 9 and 14.5 ms, respectively, which are much slower times than our nonpolar GaN MSM-PD and are similar to other *c*-plane MSM-PD results.[14,15] This further confirms the major advantages of nonpolar GaN.

■ CONCLUSION

In conclusion, a nonpolar GaN MSM-PD with superior performance has been reported, exhibiting an extremely high responsivity of 695.3 A/W at 1 V bias and 12628.3 A/W at 5 V bias, both under 360 nm UV illumination, which are more than 20 times higher and 4 orders of magnitude higher compared to those of the current state-of-the art device, respectively. The rise time and the fall time of our MSM-PD are 66 and 43 μs, which are 3 orders of magnitude faster than those of the current state-of-the-art nonpolar GaN PDs. The superior performance is attributed to our nonpolar $(11\bar{2}0)$ GaN stripe arrays with a major improvement in crystal quality grown on patterned (110) silicon substrates, which has been proved by detailed XRD and low-temperature PL measurements.

■ METHODS

Pattern Template Fabrication. A 200 nm SiO_2 thin film is initially prepared on a precleaned (110) Si substrate by plasma-enhanced chemical vapor deposition (PECVD). A periodic stripe pattern is then transferred onto the SiO_2 mask by using a standard photolithography technique. Subsequently, a standard reactive-ion etching (RIE) technique is used to etch the SiO_2 layer into 4-μm open windows separated by 4 μm wide SiO_2 masks, where the RIE etching is performed by using etchant gas CHF_3 with a flow rate of 35 standard cubic centimeters per minute (sccm) at 90 W RF power under 35 mTorr pressure. Subsequently, an anisotropic chemical etching process is conducted by merging the (110) Si substrate with the patterned SiO_2 masks into a KOH solution (25 wt %). Finally, all the SiO_2 masks on top of the (110) facet are removed by 40% buffered HF.

Epitaxial Growth. The template is initially subject to an annealing process in pure hydrogen ambient at 1310 °C for 900 s. GaN is subsequently grown at 1300 °C for 300−500 s, followed by further GaN growth conducted at 1200 °C for 7000 s to achieve a flat top surface, where the optimized flow rates of NH_3 and TMGa (Ga precursor) are 300 and 40 sccm, respectively, with a V/III ratio of 136. Other V/III ratios and temperatures are also tried (see Table S1 in the Supporting Information).

X-ray Diffraction Rocking Curve Measurements. Because of the anisotropic nature of $(11\bar{2}0)$ GaN, the fwhm of XRD rocking curves as a function of azimuthal angle has been measured, where the zero azimuthal angle is along the projection of the incident beam when it is parallel to the *c*-direction of the epilayer.

Photodetector Measurements. Photoresponsivity measurements have been carried out by a standard photoresponse testing system, which is equipped with a calibrated Hamamatsu xenon lamp, a SPEX 1681 Monochromator, and a Keithley 2400 source meter. For response-time measurements, an oscilloscope (DSO-X200A) with a bandwidth of 70 MHz and a sampling rate of 2 GSa/s is employed to measure the voltage waveform on the load resistor. The response waveform of our MSM-PD is recorded by the oscilloscope, and the response time is extracted by fitting (see Figure S1 in the Supporting Information).

■ ASSOCIATED CONTENT

ⓢ Supporting Information

The Supporting Information is available free of charge at https://pubs.acs.org/doi/10.1021/acsami.0c04890.

Additional material including details from a standard exponential method to extract the rise time and fall time of our nonpolar photodetectors and detailed growth conditions for our nonpolar GaN on patterned (110) silicon substrates (PDF)

■ AUTHOR INFORMATION

Corresponding Author

Tao Wang − *Department of Electronic and Electrical Engineering, The University of Sheffield, Sheffield S1 3JD, United Kingdom;* ⓞ orcid.org/0000-0001-5976-4994; Email: t.wang@sheffield.ac.uk

Authors

Yuefei Cai − *Department of Electronic and Electrical Engineering, The University of Sheffield, Sheffield S1 3JD, United Kingdom;* ⓞ orcid.org/0000-0002-2004-0881

Shuoheng Shen − *Department of Electronic and Electrical Engineering, The University of Sheffield, Sheffield S1 3JD, United Kingdom*

Chenqi Zhu − *Department of Electronic and Electrical Engineering, The University of Sheffield, Sheffield S1 3JD, United Kingdom*

Xuanming Zhao − *Department of Electronic and Electrical Engineering, The University of Sheffield, Sheffield S1 3JD, United Kingdom*

Jie Bai − *Department of Electronic and Electrical Engineering, The University of Sheffield, Sheffield S1 3JD, United Kingdom;* ⓞ orcid.org/0000-0002-6953-4698

Complete contact information is available at:
https://pubs.acs.org/10.1021/acsami.0c04890

Author Contributions

[#]Y.C. and S.S. contributed equally to this work. T.W. conceived the idea and organized the project. Y.C. fabricated devices and performed device characterization. S.S. fabricated patterned silicon substrates and contributed to material characterization. C.Z., S.S., and Y.C. grew the samples. J.B. contributed to device testing. T.W. and Y.C. prepared the manuscript.

Notes

The authors declare no competing financial interest.

■ ACKNOWLEDGMENTS

■ REFERENCES

(1) Guo, F.; Yang, B.; Yuan, Y.; Xiao, Z.; Dong, Q.; Bi, Y.; Huang, J. A Nanocomposite Ultraviolet Photodetector Based on Interfacial Trap-Controlled Charge Injection. *Nat. Nanotechnol.* **2012**, *7*, 798−802.

(2) Lubin, D.; Jensen, E. H. Effects of Clouds and Stratospheric Ozone Depletion on Ultraviolet Radiation Trends. *Nature* **1995**, *377*, 710−713.

(3) Crefcoeur, R. P.; Yin, R.; Ulm, R.; Halazonetis, T. D. Ultraviolet-B-Mediated Induction of Protein−Protein Interactions in Mammalian Cells. *Nat. Commun.* **2013**, *4*, 1779.

(4) Alaie, Z.; Mohammad Nejad, S.; Yousefi, M. H. Recent Advances in Ultraviolet Photodetectors. *Mater. Sci. Semicond. Process.* **2015**, *29*, 16−55.

(5) Muñoz, E.; Monroy, E.; Pau, J.; Calle, F.; Omnès, F.; Gibart, P. III Nitrides and UV detection. *J. Phys.: Condens. Matter* **2001**, *13*, 7115−7137.

(6) Sang, L.; Liao, M.; Sumiya, M. A Comprehensive Review of Semiconductor Ultraviolet Photodetectors: from Thin Film to One-Dimensional Nanostructures. *Sensors* **2013**, *13*, 10482−10518.

(7) Khan, S.; Newport, D.; Le Calvé, S. Gas Detection Using Portable Deep-UV Absorption Spectrophotometry: A Review. *Sensors* **2019**, *19*, 5210.

(8) Chen, R.-S.; Chen, H.-Y.; Lu, C.-Y.; Chen, K.-H.; Chen, C.-P.; Chen, L.-C.; Yang, Y.-J. Ultrahigh Photocurrent Gain in m-axial GaN Nanowires. *Appl. Phys. Lett.* **2007**, *91*, 223106.

(9) Mukundan, S.; Roul, B.; Shetty, A.; Chandan, G.; Mohan, L.; Krupanidhi, S. B. Enhanced UV Detection by Non-Polar Epitaxial GaN Films. *AIP Adv.* **2015**, *5*, 127208.

(10) Pant, R. K.; Singh, D. K.; Roul, B.; Chowdhury, A. M.; Chandan, G.; Nanda, K. K.; Krupanidhi, S. B. Photodetection Properties of Nonpolar a-Plane GaN Grown by Three Approaches Using Plasma-Assisted Molecular Beam Epitaxy. *Phys. Status Solidi A* **2019**, *216*, 1900171.

(11) Pant, R.; Shetty, A.; Chandan, G.; Roul, B.; Nanda, K. K.; Krupanidhi, S. B. In-Plane Anisotropic Photoconduction in Nonpolar Epitaxial A-Plane GaN. *ACS Appl. Mater. Interfaces* **2018**, *10*, 16918−16923.

(12) Gundimeda, A.; Krishna, S.; Aggarwal, N.; Sharma, A.; Sharma, N. D.; Maurya, K. K.; Husale, S.; Gupta, G. Fabrication of Non-Polar GaN Based Highly Responsive and Fast UV Photodetector. *Appl. Phys. Lett.* **2017**, *110*, 103507.

(13) Wang, W.; Zheng, Y.; Li, X.; Li, Y.; Huang, L.; Li, G. High-Performance Nonpolar A-Plane GaN-Based Metal−Semiconductor−Metal UV Photo-Detectors Fabricated on LaAlO₃ Substrates. *J. Mater. Chem. C* **2018**, *6*, 3417−3426.

(14) Mukundan, S.; Mohan, L.; Chandan, G.; Roul, B.; Krupanidhi, S. B. Semipolar and Nonpolar GaN Epi-films Grown on M-Sapphire by Plasma Assisted Molecular Beam Epitaxy. *J. Appl. Phys.* **2014**, *116*, 204502.

(15) Ren, B.; Liao, M.; Sumiya, M.; Huang, J.; Wang, L.; Koide, Y.; Sang, L. Vertical-Type Ni/GaN UV Photodetectors Fabricated on Free-Standing GaN Substrates. *Appl. Sci.* **2019**, *9*, 2895.

(16) Sun, X.; Li, D.; Li, Z.; Song, H.; Jiang, H.; Chen, Y.; Miao, G.; Zhang, Z. High Spectral Response of Self-Driven GaN-Based Detectors by Controlling the Contact Barrier Height. *Sci. Rep.* **2015**, *5*, 16819.

(17) Jain, S. K.; Aggarwal, N.; Krishna, S.; Kumar, R.; Husale, S.; Gupta, V.; Gupta, G. GaN-UV Photodetector Integrated with Asymmetric Metal Semiconductor Metal Structure for Enhanced Responsivity. *J. Mater. Sci.: Mater. Electron.* **2018**, *29*, 8958−8963.

(18) Yan, R.; Gargas, D.; Yang, P. Nanowire Photonics. *Nat. Photonics* **2009**, *3*, 569−576.

(19) Tchernycheva, M.; Messanvi, A.; de Luna Bugallo, A.; Jacopin, G.; Lavenus, P.; Rigutti, L.; Zhang, H.; Halioua, Y.; Julien, F. H.; Eymery, J.; Durand, C. Integrated Photonic Platform Based on InGaN/GaN Nanowire Emitters and Detectors. *Nano Lett.* **2014**, *14*, 3515−3520.

(20) Ni, X.; Wu, M.; Lee, J.; Li, X.; Baski, A. A.; Özgür, Ü.; Morkoç, H. Nonpolar M-Plane GaN on Patterned Si (112) Substrates by Metalorganic Chemical Vapor Deposition. *Appl. Phys. Lett.* **2009**, *95*, 111102.

(21) Ding, K.; Avrutin, V.; Izyumskaya, N.; Metzner, S.; Bertram, F.; Christen, J.; Ozgur, U.; Morkoc, H. Recent Progress in Nonpolar and Semi-Polar GaN Light Emitters on Patterned Si Substrates. *Proceedings, Gallium Nitride Materials and Devices XIII* **2018**, *10532*, 1053208.

(22) Kim, M.; Do, Y.; Kang, H.; Noh, D.; Park, S. Effects of Step-Graded AlxGa1-xN Interlayer on Properties of GaN Grown on Si (111) Using Ultrahigh Vacuum Chemical Vapour Deposition. *Appl. Phys. Lett.* **2001**, *79*, 2713−2715.

(23) Cai, Y.; Zhu, C.; Jiu, L.; Gong, Y.; Yu, X.; Bai, J.; Esendag, V.; Wang, T. Strain Analysis of GaN HEMTs on (111) Silicon with Two Transitional AlxGa1-xN Layers. *Materials* **2018**, *11*, 1968.

(24) Zhang, Y.; Bai, J.; Hou, Y.; Smith, R. M.; Yu, X.; Gong, Y.; Wang, T. Defect Reduction in Overgrown Semi-Polar (11−22) GaN on A Regularly Arrayed Micro-Rod Array Template. *AIP Adv.* **2016**, *6*, 025201.

(25) Jiu, L.; Gong, Y.; Wang, T. Overgrowth and Strain Investigation of (11−20) Non-Polar GaN on Patterned Templates on Sapphire. *Sci. Rep.* **2018**, *8*, 9898.

(26) Cai, Y.; Yu, X.; Shen, S.; Zhao, X.; Jiu, L.; Zhu, C.; Bai, J.; Wang, T. Overgrowth and Characterization of (11−22) Semi-Polar GaN on (113) Silicon with A Two-Step Method. *Semicond. Sci. Technol.* **2019**, *34*, 045012.

(27) Wang, T. Topical Review: Development of Overgrown Semi-Polar GaN for High Efficiency Green/Yellow Emission. *Semicond. Sci. Technol.* **2016**, *31*, 093003.

(28) Gühne, T.; Bougrioua, Z.; Laügt, S.; Nemoz, M.; Vennéguès, P.; Vinter, B.; Leroux, M. Band-Edge Photoluminescence and Reflectivity of Nonpolar (11−20) and Semipolar (11−22) GaN Formed by Epitaxial Lateral Overgrowth on Sapphire. *Phys. Rev. B: Condens. Matter Mater. Phys.* **2008**, *77*, 075308.

(29) Lee, C.; Won, C.; Lee, J.; Hahm, S.; Park, H. Selectively Enhanced UV-A Photo Responsivity of A GaN MSM UV Photo-detector with A Step-Graded AlxGa1-xN Buffer Layer. *Sensors* **2017**, *17*, 1684.

(30) Munoz, E.; Monroy, E.; Garrido, J. A.; Izpura, I.; Sánchez, F. J.; Sánchez-García, M. A.; Calleja, E.; Beaumont, B.; Gibart, P. Photoconductor Gain Mechanisms in GaN Ultraviolet Detectors. *Appl. Phys. Lett.* **1997**, *71*, 870.